Magnetic structure of $Co_{1/3}NbS_2$ and $Co_{1/3}TaS_2$

1983 J. Phys. C: Solid State Phys. 16 2765

(http://iopscience.iop.org/0022-3719/16/14/016)

J. Phys. C: Solid State Phys., **16** (1983) 2765–2778. Printed in Great Britain

Magnetic structure of $Co_{1/3}NbS_2$ and $Co_{1/3}TaS_2$

S S P Parkin†‡, E A Marseglia† and P J Brown§

† The Cavendish Laboratory, Madingley Road, Cambridge, UK

§ Institut Laue–Langevin, 156 X Centre de Tri, 38042 Grenoble Cedex, France

Received 24 November 1982

Abstract. We have examined the magnetic structures of the antiferromagnetic layered compounds $Co_{1/3}NbS_2$ and $Co_{1/3}TaS_2$ using single-crystal neutron photographic and counting methods. The magnetic structure of $Co_{1/3}NbS_2$ has been determined in detail, and has an orthohexagonal unit cell, containing two Co atoms, arranged on the 'hexagonal ordering of the first kind' scheme. The different symmetries of the crystallographic and magnetic unit cells leads to a complicated domain structure. A large part of the magnetisation in this material is localised on the Co atoms, although the magnetic moment of the Co^{2+} ion is ~10% lower than that of the corresponding spin-only moment. The magnetic structure of the related material, $Co_{1/3}TaS_2$, which has the same crystal structure as $Co_{1/3}NbS_2$, is very different, and is a triangular antiferromagnetic structure although for this material only the unit cell has been determined.

1. Introduction

The 3d transition-metal intercalates of the niobium and tantalum dichalcogenides form an isostructural family of magnetic metals which display a fascinating complexity of magnetic behaviour, including both ferromagnetic and antiferromagnetic orderings at low temperatures (Parkin and Friend 1980a, b, and references therein). The crystallographic structure of these materials is based on the 2H polytype structure of the corresponding host layered transition-metal dichalcogenide (TMDC) with the 3d transition metal occupying some fraction of the octahedral sites between the TMDC layers (figure 1). Ordered arrays of the intercalate atoms are found for concentrations of $\frac{1}{3}$ and $\frac{1}{4}$ corresponding, respectively to $3^{1/2} \times 3^{1/2}$ and 2×2 superlattices. Although it is possible to grow material with intermediate intercalate concentrations, such materials are not single-phase compounds and, in general, show both $3^{1/2} \times 3^{1/2}$ and 2×2 superlattices (Le Blanc-Soreau *et al* 1976). Our studies have been concerned only with single-phase single-crystal materials with stoichiometries close to $\frac{1}{3}$ or $\frac{1}{4}$.

The crystal structure of the layered intercalate compounds gives rise to some unusual magnetic and transport properties, in that there are essentially two subsystems of electrons—those localised on the intercalate ions between the layers, and those delocalised within the TMDC layers forming a partially filled conduction band associated primarily with the Nb and Ta d levels. Optical and transport measurements show that two or three electrons per intercalate ion are transferred to the initially half-filled

‡ Present address: IBM Research Laboratory, 5600 Cottle Road, K32/281, San Jose, CA 95193, USA.

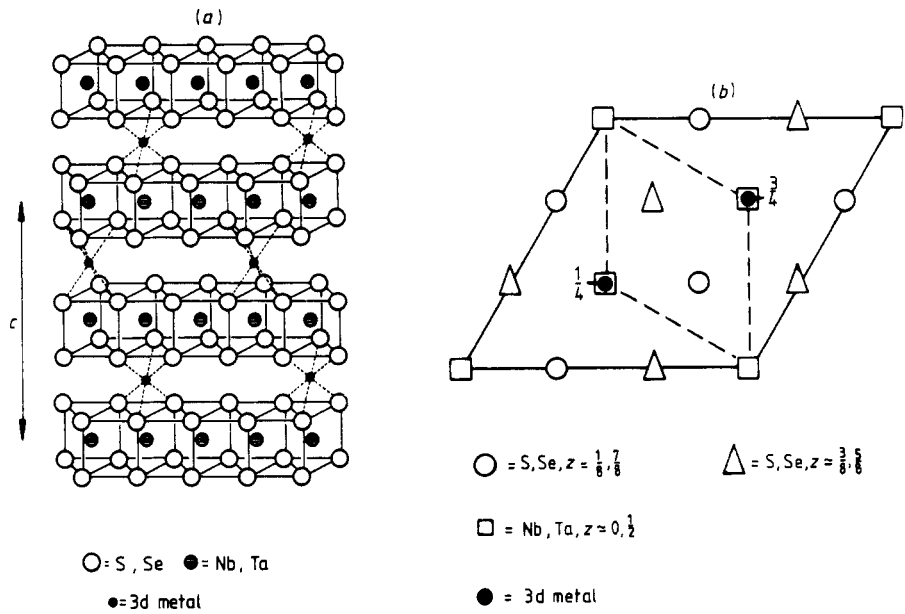

Figure 1. (*a*) Structure of the 3d intercalation complexes, $M_{1/3}TX_2$ (M = 3d transition metal; T = Nb or Ta; X = S or Se). (*b*) Projection of the structure of $M_{1/3}TX_2$ onto the plane (001), showing the $3^{1/2} \times 3^{1/2}$ superlattice formed.

conduction band of the host TMDC. Valence states of 3+ for the V and Cr intercalate ions and 2+ for the Mn, Fe, Co and Ni ions for various host materials can be assigned unambiguously to these species from the position of the Drude edge in optical reflectivity measurements (Parkin and Beal 1980) and the magnitude of the room-temperature Hall coefficient (Parkin and Friend 1980b) and by considering the variation of such physical

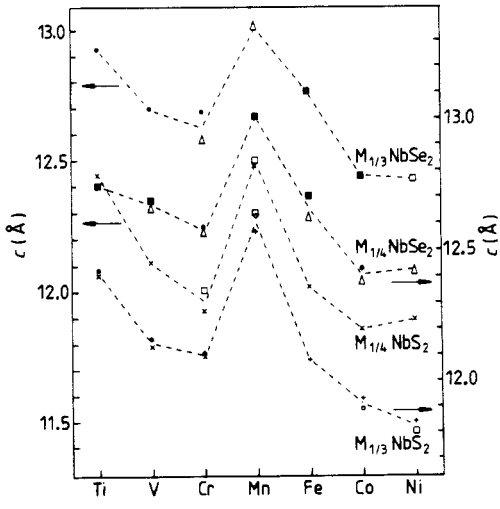

Figure 2. Lattice parameter perpendicular to the layers, *c*, plotted against M for the complexes M_xNbS_2 and M_xNbSe_2 for $x = \frac{1}{3}$ and $\frac{1}{4}$ (after Parkin 1980).

properties as the electrical resistivity and the TMDC layer–layer separation (characterised by the c lattice parameter) as the intercalate ion is varied from V to Ni (Friend *et al* 1977, Parkin and Friend 1980a) for the $\frac{1}{3}$-concentration complexes of NbS_2 and TaS_2. The same valence states for the various 3d intercalate ions for other intercalation complexes are suggested by similar variations of the lattice parameter c: figure 2 shows data for the $\frac{1}{3}$- and $\frac{1}{4}$-concentration complexes of NbS_2 and $NbSe_2$. The jump in the lattice parameter c between the Cr and Mn compounds corresponds to a decreased electrostatic coupling between the layers and the intercalate ions as the valence state changes from 3+ in Cr to 2+ in the Mn compounds. The remaining electrons on the divalent or trivalent ions are localised and form magnetic moments. Recent single-crystal magnetic susceptibility measurements show that for several V, Cr and Mn intercalates, the measured Curie–Weiss moment is in reasonable agreement with the spin-only moment of the corresponding ion, with the valence states mentioned above (Parkin and Friend 1980a). The orbital contribution to the moment is quenched by the crystal fields, except for $Fe_{1/3}NbS_2$ and $Fe_{1/3}TaS_2$ in which cases the magnetic moment, as a result of the orbital contribution, is significantly larger than the spin-only moment of Fe^{2+} (Friend *et al* 1977, Parkin and Friend 1980a). Note that much of the early work on these materials consisted of a determination of the magnetic moments from susceptibility measurements, but that since many of these studies were made on powders of ill defined stoichiometry, these results are not very useful (for a review, see van den Berg 1976).

Perhaps the most interesting aspect of these materials is the interaction of the localised electrons on the 3d ions and the conduction electrons. Transport and optical measurements suggest an important interaction between these two subsystems leading to a broadening of the conduction band of the corresponding host material and the formation of virtually broadened 3d states (Parkin and Friend, 1980b, Parkin and Beal 1980, Parkin and Bayliss 1982). The strength of this coupling can be probed via measurements of the spin-disorder resistivity, ρ_{sd}, and the position of features in the optical reflectivity spectra. These independent measurements show a similar variation of the interaction strength as the intercalate ion is varied in a given host compound. The interaction is weaker at the beginning, middle and end of the period with larger values for the Cr and Fe intercalates.

Previous work to determine the nature of the magnetic ordering at low temperatures consists of powder neutron diffraction studies by van Laar *et al* (1971) at 4.2 K and directional single-crystal magnetic susceptibility measurements by Eibschutz *et al* (1975), Friend *et al* (1977) and Parkin and Friend (1980a). Parkin and Friend (1980a) have shown that for the $\frac{1}{3}$-concentration NbS_2 and TaS_2 complexes, the V, Cr and Mn complexes all show ferromagnetic behaviour, whereas the Co and Ni intercalates all show antiferromagnetic behaviour. The Fe intercalates form an intermediate case and show both ferromagnetic and antiferromagnetic orderings, depending on the host compound. The systematic change in the type of magnetic behaviour as the intercalate species is vaired across the periodic table can be understood in terms of competing superexchange and RKKY interactions (Parkin and Friend 1980a). Determination of the low-temperature structure of these materials is important in order to gain a more complete understanding of their magnetic behaviour, particularly with respect to the antiferromagnetic complexes. The only structural work consists of that by van Laar *et al* (1971), who carried out powder neutron diffraction studies at 4.2 K on several Mn complexes which are ordered ferromagnetically within the hexagonal layers and two antiferromagnetic compounds, $Fe_{1/3}NbS_2$ and $Cr_{1/4}NbS_2$. These compounds adopt different magnetic structures. $Fe_{1/3}NbS_2$ adopts a complicated structure known as hexagonal ordering of the

third kind. The moment of each Fe ion is aligned antiparallel to 8 of its 12 nearest neighbours and parallel to the remaining 4: the moments are aligned along the *c* axis. On the other hand, $Cr_{1/4}NbS_2$ takes up a simpler structure in which ferromagnetic planes of Cr atoms are coupled antiferromagnetically along the *c* axis. This structure is termed a hexagonal ordering of the second kind by Corliss *et al* (1956) and a hexagonal type II structure by Goodenough (1963). However, van Laar *et al* (1971) emphasise that for this complex they find only a few very weak magnetic reflections.

Also, van Laar *et al* (1971) made measurements on the compound of interest here, $Co_{1/3}NbS_2$, but were not able to index the large number of very weak reflections they observed at 4.2 K. In this paper we report the determination of the magnetic structure of $Co_{1/3}NbS_2$ at 4.2 K through single-crystal neutron diffraction measurements, using both photographic and counting techniques. This compound orders antiferromagnetically below a Néel temperature of ~25 K; the temperature dependence of the magnetisation below T_N is unusual with the development along *c* of a residual ferromagnetic moment depending on the magnetic field applied during cooling (Friend *et al* 1977). This behaviour has been examined in more detail recently with both a vibrating-sample magnetometer and a SQUID magnetometer, confirming the effect and establishing the existence of some compensation temperature where the zero-field magnetisation goes to zero (Parkin *et al* 1983a). These observations were an important motivation for a detailed examination of the magnetic structure of this compound.

2. Experimental details

Neutron diffraction data have been collected on single crystals of $Co_{1/3}NbS_2$ and $Co_{1/3}TaS_2$, although only incomplete measurements have been made on the latter compound. Preliminary data were taken on the Mark VI two-circle diffractometer at the Atomic Energy Research Establishment (Harwell) and, subsequently, measurements were made on crystals of $Co_{1/3}NbS_2$ with the low-temperature neutron Weissenberg camera (the D12 instrument) and the $2\frac{1}{2}$ circle D15 diffractometer at the Institut Laue–Langevin, Grenoble.

Crystals of $Co_{1/3}TaS_2$ were taken from the same batch as that used by Parkin and Friend (1980a, b). The crystals of $Co_{1/3}NbS_2$ used were specially grown for these experiments in order to provide large single crystals. The resistance ratio of these samples is about 7, somewhat larger than that measured on a previous batch of crystals ($\simeq$4) grown in the same way, and on which some magnetic and transport measurements have been reported (Friend *et al* 1977, Parkin and Beal 1980). A higher resistance ratio implies better crystal quality and a stoichiometry closer to ideal (Le Blanc-Soreau *et al* 1976). For both Co intercalates, room-temperature x-ray measurements reveal the presence of a single superlattice, the $3^{1/2} \times 3^{1/2}$ superstructure, indicating that the Co concentration is close to $\frac{1}{3}$ and that these materials are single-phase compounds. Indeed the structural measurements on $Co_{1/3}NbS_2$ presented below show that the Co concentration is to within 5% of $\frac{1}{3}$.

The crystals of $Co_{1/3}TaS_2$ and $Co_{1/3}NbS_2$ used measured approximately $7 \times 10 \times 3$ and $4 \times 5 \times 3$ mm^3 respectively. Absorption corrections were estimated as being no greater than 15% for $Co_{1/3}TaS_2$ and 4% of the incident neutron beam for $Co_{1/3}NbS_2$ (using absorption coefficients tabulated by Bacon (1975) and corrected for the wavelength of 1.176 Å used for the D15 experiments).

2.1. Neutron photographs

The design of the D12 instrument at the ILL is similar to that of a conventional x-ray Weissenberg camera rotated through 90°, but with modifications to allow for the fitting of a low-temperature cryostat with an aluminium tail (Hohlwein and Wright 1981). Scattering from the cryostat tail is absorbed by radial screens, in the form of a 'cylindrical venetian blind', which are oscillated about the tail (Wright *et al* 1981). Reflections are recorded on photographic film by means of conversion scintillators between which the film is tightly sealed. This instrument has all the advantages associated with photographic detection and, in particular, enables large areas of reciprocal space to be scanned, thus allowing much more efficient determination of superlattices than conventional diffractometers. This technique is especially suited to the measurement of weak reflections. For the experiments on $Co_{1/3}NbS_2$, exposure times of about 40 h were required. Both oscillation and Weissenberg photographs were taken.

2.2. Diffractometer measurements

Preliminary measurements were made on the Mark VI diffractometer at the AERE (Harwell), and the antiferromagnetic unit cells of both $Co_{1/3}NbS_2$ and $Co_{1/3}TaS_2$ were determined by considering various possible structures and making scans along certain directions in reciprocal space. For $Co_{1/3}TaS_2$, the magnetic intensities were very weak and only about two to three times as large as the background intensity; for $Co_{1/3}NbS_2$, the most intense reflection was only ten times the background. The scope of these experiments was therefore severely limited since the scan time for each reflection had to be of the order of 2 h to obtain reasonable statistics.

Detailed measurements on $Co_{1/3}NbS_2$ were later made at the ILL, Grenoble. Scan times were considerably shorter and of the order of 2–3 min. Integrated intensities were recorded using $\theta/2\theta$ scans.

3. Results

3.1. $Co_{1/3}NbS_2$

3.1.1. Determination of the magnetic unit cell. Antiferromagnetic structures are necessarily complicated in systems of hexagonal symmetry. For such systems, the most commonly found magnetic structures are the collinear ones based on an orthohexagonal supercell, one of which is found, for example, in the hexagonal polymorph of β-MnS (Corliss *et al* 1956), the collinear type II hexagonal structure described above for $Cr_{1/4}NbS_2$, and more complicated non-collinear structures such as the triangular antiferromagnetic structure found in the rare-earth manganites, $RMnO_3$ where R = rare earth (Bertaut and Mercier 1963, Bertaut *et al* 1967) and the related 'umbrella structure' found in CrSe (Corliss *et al* 1961). For the preliminary single-crystal diffractometer experiments at Harwell, several non-equivalent reflections containing only a magnetic neutron scattering contribution were calculated on the basis of the various models outlined above, and these reflections were scanned. Magnetic reflections, confirmed by checking the scattered intensity dropped to zero above the Néel temperature, were found that could be indexed on an orthohexagonal cell with a volume twice that of the crystallographic unit cell. About 25 magnetic reflections were measured and it was found that these were in qualitative agreement with the orthohexagonal structure named

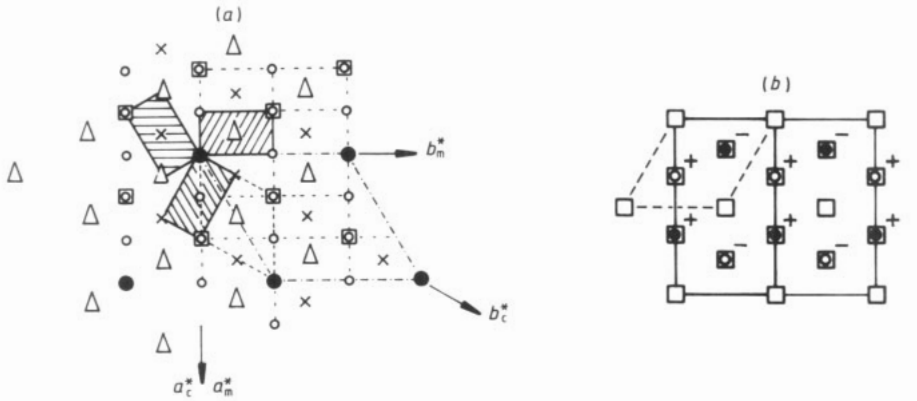

Figure 3. (*a*) Projection of the magnetic and crystallographic reciprocal lattices of $Co_{1/3}NbS_2$ onto the $hk0$ plane. ■ = 2H NbS_2 reciprocal lattice with parameters, $a_h^* = b_h^* = 3^{1/2}a_c^*$, where a_c^* (and b_c^*) correspond to the $Co_{1/3}NbS_2$ superlattice; □ = $3^{1/2} \times 3^{1/2}$ $Co_{1/3}NbS_2$ reciprocal lattice; ○, △, × = the three distinct magnetic reciprocal lattices for which $a_m^* = \frac{1}{2}a_c^*$ and $b_m^* = \frac{1}{2}3^{1/2}a_c^*$. The unit cells describing the three magnetic lattices are shown cross-hatched. (*b*) Arrangement of Co spins corresponding to the structure 'hexagonal ordering of the first kind', + and − refer to moments aligned respectively parallel and antiparallel to some axis. The primitive magnetic unit cell is shown in full lines. The crystallographic unit cell is shown as broken lines. □ = Nb, $z \simeq 0, \frac{1}{2}$; ○ = Co, $z \simeq \frac{1}{4}$; ● = S, $z \simeq \frac{3}{4}$.

'hexagonal ordering of the first kind' by Corliss *et al* (1956), although no quantitative comparison could be made because of the limited data set. As discussed below, later measurements made at the ILL are in good quantitative agreement with this particular structure, confirming these results.

An interesting consequence of the different symmetries of the magnetic and crystallographic lattices is the possibility of observing experimentally different magnetic domains. As is illustrated in figure 3, there are three ways in which the orthohexagonal magnetic lattice can be accommodated within the hexagonal crystallographic lattice,

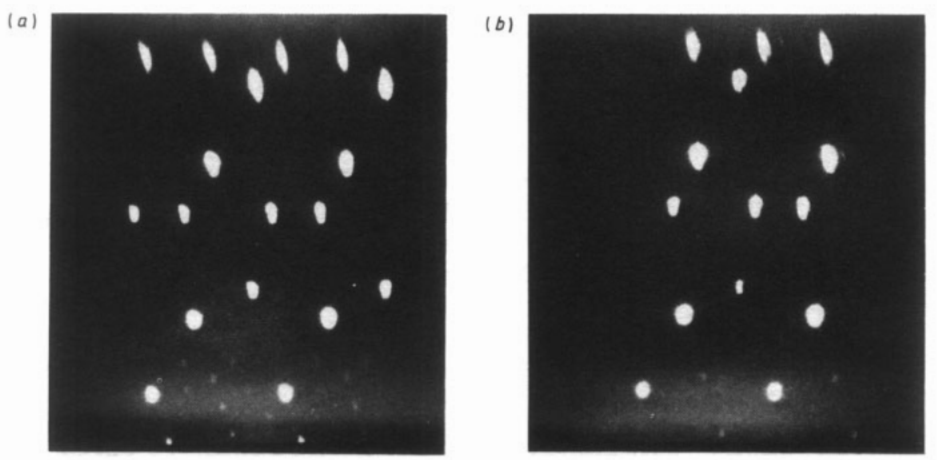

Figure 4. Zero-layer *c* axis neutron Weissenberg photographs of $Co_{1/3}NbS_2$ taken at (*a*) 4.2 and (*b*) 60 K.

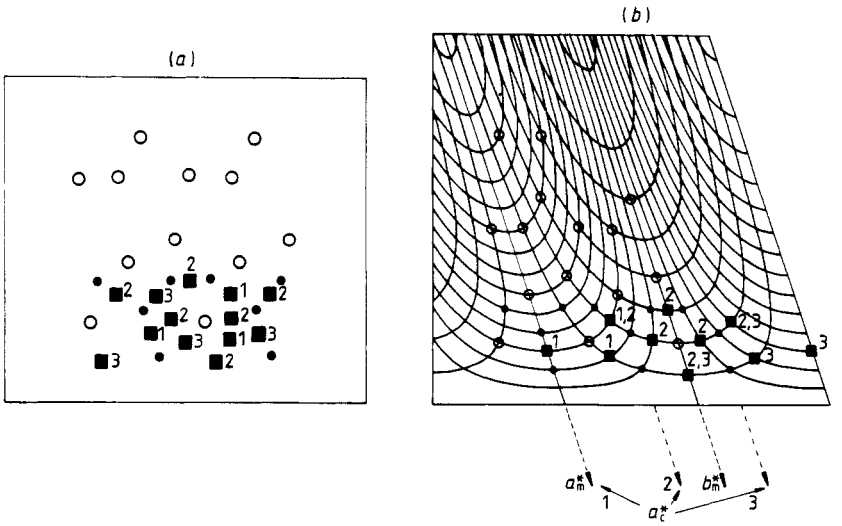

Figure 5. (*a*) The low-angle region of the Weissenberg $3^{1/2} \times 3^{1/2}$ graph shown in figure 4(*a*) showing reflections from: ○, the 2H NbS_2 lattice; ●, the 3 × 3 Co crystallographic superlattice; ■, the orthohexagonal magnetic superlattice. The labels 1, 2, 3, correspond to reflections from the three configurational domains (see figure 5(*b*)). (*b*) A part of the *hk*0 Weissenberg chart for the magnetic superlattice found in $Co_{1/3}NbS_2$. a_m^* and b_m^* are the magnetic reciprocal-lattice axes which are 90° apart. a_c^*, the crystallographic reciprocal-lattice axis, can take up any one of the three positions, at 60° to each other, that are labelled 1, 2 and 3. Correspondingly the magnetic reflections are labelled 1, 2 or 3, according to where the a_c^* axis must be placed to accommodate the reflection on the chart and thus correspond to the different domains shown in figure 5(*a*).

which gives rise to three distinct sets of magnetic reflections in reciprocal space, none of which overlap except where there is also a nuclear scattering contribution. We have observed reflections corresponding to each of these configurational domains and have found that equivalent reflections are of the same intensity. Note that within each of these configurational domains, the moments can be aligned along several symmetry-related directions, giving rise to spin domains that cannot be separately distinguished.

Zero-layer Weissenberg pictures of a single crystal of $Co_{1/3}NbS_2$ taken on the D12 instrument at Grenoble with the *c* axis along the rotation axis are shown in figure 4 corresponding to temperatures of 4 and 60 K. An exposure time of 40 h was used for each photograph with rotation of the crystal through approximately 120°. The reflections seen in the photographs are analysed in figure 5. The very intense reflections are highly over-exposed and correspond to nuclear reflections from the host 2H NbS_2 lattice. Much weaker reflections can be seen in figure 4 at low Bragg angles near the forward beam. Some of the weak reflections seen at 4 K in figure 4(*a*) are absent in figure 4(*b*) at 60 K, which is well above the Néel temperature (≃25 K) and can therefore be associated with scattering from the ordered antiferromagnetic superlattice. The weak reflections seen at both 4 and 60 K correspond to scattering from the $3^{1/2} \times 3^{1/2}$ crystallographic superlattice of Co atoms. Figure 5(*a*) shows the low-angle region of the low-temperature photograph in figure 4 and distinguishes the various magnetic and nuclear lattice contributions. Figure 5(*b*) shows a part of the Weissenberg net for an orthorhombic lattice with a unit cell corresponding to that of the magnetic lattice in $Co_{1/3}NbS_2$ found above, and illustrates the various ways in which the magnetic and crystallographic lattices can

be accommodated. The figure shows how it is possible to account for all the reflections seen in figure 4 by including the three configurational magnetic domains.

3.1.2. Determination of the magnetic structure. The size of the magnetic moment of the cobalt intercalate ion can be determined from the measured intensities of the magnetic reflections at low temperatures by normalising these with respect to those of the nuclear reflections. Data for the nuclear structure were collected both at room temperature and at 4.2 K. After averaging over equivalent reflections, 78 independent nuclear structure factors were obtained at room temperature for the unit cell of the $3^{1/2} \times 3^{1/2}$ superlattice structure. The room-temperature nuclear structure of $Co_{1/3}NbS_2$ has previously been determined by both single-crystal x-ray diffraction and powder neutron diffraction experiments (Anzenhofer *et al* 1970, van Laar *et al* 1971). Our data are in good agreement with these measurements which showed the space group of $Co_{1/3}NbS_2$ to be $P6_322$ with the cobalt atoms occupying the 2c sites. A least-squares structural refinement of our data gave the parameters shown in table 1 with a low *R*-factor of only 0.07%, but with the three most intense reflections (all about 60% larger than the next most intense reflections) eliminated from the data set because of effects of extinction observed for these reflections. If these data are retained, reasonable values for some of the parameters, and in particular, the Co isotropic temperature factor (ITF) and site-occupation factor (SOF) cannot be obtained and the *R*-factor is about 100 times larger. No attempt was made to correct for this effect apart from eliminating certain reflections as mentioned above. Anzenhofer *et al* (1970) have previously reported observing primary extinction in crystals of $M_{1/3}NbS_2$ compounds.

Table 1. Room-temperature structural parameters for $Co_{1/3}NbS_2$. Other parameters: lattice parameters: $a = 5.749$ Å, $c = 11.886$ Å; neutron nuclear scattering factors: Co(0.278), Nb((0.7050), S(0.2847) $\times 10^{-12}$ cm; atomic positions and number of atoms in unit cell: 2Co (2c), $\frac{1}{3}$, $\frac{2}{3}$, $\frac{1}{4}$; 2Nb (2a), 0, 0, 0; 4Nb (4f), $\frac{1}{3}$, $\frac{2}{3}$, z: $z \simeq 0$; 12S (12i), x, y, z: $x \simeq \frac{1}{3}$, $y \simeq 0$, $z \simeq \frac{3}{8}$.

s (12i)			Co (2c)		Nb (4f)	Nb	S
x	y	z	SOF	ITF	z	ITF	ITF
0.3322 (0.0003)	0.0009 (0.0003)	0.3694 (0.0005)	0.949 (0.0273)	0.0182 (0.0807)	0.9944	0.01	0.02

A preliminary refinement was carried out to obtain our approximate value for the ITF of the Nb and S atoms with other parameters fixed. Note that following the work of Anzenhofer *et al* (1970), the Co atoms were only allowed to fill the 2c sites and that there is a high correlation between the Co ITF and SOF, giving rise to the large uncertainties in these parameters. Values of the neutron nuclear scattering factors (NSF) used are shown in table 1. A value of 0.278 for the Cc coherent scattering factor as recently determined by Koester *et al* (1974) has been used. Previously a value of 0.25 for this factor was widely accepted (Bacon 1975) and was presumably used by van Laar *et al* (1971), so considerably affecting the values of, in particular, the Co occupation site factor that they determined. Using the lower value of 0.25 instead of 0.278 would increase the SOF by about 11%. Our measurements give, for the crystal of $Co_{1/3}NbS_2$ used here, a Co SOF for the 2c site of 0.95, thus corresponding to a Co deficiency of only 5%. This, taken together with the

observation of extinction on the most intense nuclear reflections, suggests high crystal quality.

Measurements of both magnetic and nuclear reflections were made at 4.2 K. The magnetic reflections scanned were those corresponding to the magnetic unit cell determined above, which has a volume twice that of the crystallographic unit cell and contains four Co atoms. About 30 non-equivalent sets of magnetic reflections were measured for each of the three configurational magnetic domains described above. No significant difference between the intensities of equivalent reflections for different domains was found. All possible arrangements of the Co magnetic moments consistent with the unit cell observed were considered (Corliss *et al* 1956); the arrangement of moments termed hexagonal ordering of the first kind is in good agreement with the data and is illustrated in figure 3(*b*). A least-squares fitting program was used with only two independent variables, namely the components of spin perpendicular and parallel to the layers, $S_\perp$ and $S_\parallel$, although it was found that the component of spin perpendicular to the layer was zero to within the experimental accuracy. Note that the orientation of the spin within the hexagonal layer cannot be determined for the following reason: the orientation of the spin with respect to the lattice will be determined by the local crystalline fields which have sixfold symmetry, so $S_\parallel$ can lie along any of six axes inclined at 60° with respect to one another. For a collinear antiferromagnetic structure, the magnetic scattering factor depends upon

$$q = \frac{\boldsymbol{\kappa}}{|\boldsymbol{\kappa}|}\left(\frac{\boldsymbol{\kappa}}{|\boldsymbol{\kappa}|}\cdot\boldsymbol{\eta}\right) - \boldsymbol{\eta}$$

where $\boldsymbol{\kappa}$ is the scattering vector and $\boldsymbol{\eta}$ is a unit vector along the spin direction (Brown 1978). By averaging over the various spin directions, $\boldsymbol{S}$, for a given (hkl), one finds that

$$\langle q^2\rangle = 1 - [1/(dS)^2]\tfrac{1}{2}[2S_z^2 l^2 + (S_x^2 + S_y^2)(h^2 + k^2)]$$

where d and S are the lengths of the vectors (hkl) and $\boldsymbol{S}$, respectively. Thus it is not possible to find S_x and S_y separately by varying hkl.

Measured and calculated magnetic structure factors for the model discussed above are shown in table 2. The experimental data are averaged over the three configurational domains. The R-factor is very low at 1.4%. The χ-factor

$$\chi = \frac{\sum (f_{\text{obs}} - f_{\text{cal}})^2}{\sum (\Delta f_{\text{cal}})^2}$$

is 3.5, indicating reasonable agreement with the model. The magnetic scattering factor is proportional to $p = 0.27\ \mu f_{\text{mag}} \times 10^{-14}$ m where f_{mag} is the magnetic form factor and μ is the magnetic moment ($=2S\mu_B$ where S is the spin quantum number). By normalising the magnetic intensities with respect to the nuclear intensities at low temperatures and taking into account the presence of the configurational domains and the increased size of the magnetic unit cell with respect to that of the configurational unit cell, μ can be determined if f_{mag} is known. In the fitting procedure, an expansion of f_{mag} in the form

$$f_{\text{mag}} = A\exp(-ax^2) + B\exp(-bx^2) + C$$

where $x = (\sin\theta)/\lambda$ was used with values of the parameters A, a, B, b, C taken from Lisher and Forsyth (1971) for the Co^{2+} ion. A value of $\mu = 2.60 \pm 0.05\ \mu_B$ per Co site was found. Assuming the Co SOF of 95 ± 2% found above, this corresponds to a moment per Co atom of 2.73 μ_B which can be compared with the spin-only moment for the Co^{2+}

Table 2. Magnetic structure factors at 5 K for $Co_{1/3}NbS_2$. F_{meas} and F_{cal} are the measured and calculated magnetic structure factors, as described in the text.

h	k	l	F_{meas}	F_{cal}
1	0	0	5.95	6.28
3	0	0	11.14	10.53
5	0	0	4.69	3.82
2	1	0	6.21	5.50
4	1	0	5.77	4.27
1	0	1	10.46	12.73
5	0	1	5.78	6.59
2	1	1	10.46	9.79
4	1	1	7.47	7.44
1	0	2	6.05	7.77
3	0	2	10.04	11.04
5	0	2	4.36	3.79
0	1	2	13.76	13.75
2	1	2	7.02	5.87
4	1	2	3.71	4.29
1	0	3	10.87	12.90
5	0	3	6.03	6.41
2	1	3	10.87	10.10
4	1	3	8.70	7.32
1	0	4	6.36	6.80
3	0	4	11.29	10.41
0	1	4	12.86	12.60
2	1	4	5.80	5.52
4	1	4	4.57	4.02
1	0	5	9.60	10.41
2	1	5	9.37	8.69
1	0	6	3.77	5.18
0	1	6	11.39	9.81
2	1	6	4.77	4.42

ion of $3\mu_B$. The observed moment is thus significantly lower ($\simeq$8–10%) than the Co^{2+} spin-only moment, although clearly much closer to this value than that of the Co^{1+} spin-only moment ($2\mu_B$), thus confirming a valence state of 2+ for the intercalate ion. Note that any orbital moment contribution would result in an increased magnetic moment for the Co^{2+} ion; we shall assume the orbital moment is completely quenched. (As mentioned above there is some ambiguity in the Co NSF which leads to some uncertainty in the Co SOF. In particular using the lower value of the Co NSF would increase the Co SOF and so reduce further the effective moment per Co atom to $\simeq 2.5\mu_B$ which is about 17% lower than the spin-only moment for Co^{2+}.)

The magnetic intensities were measured at 4.2 K; it is to be expected that at lower temperatures a slightly larger moment would be found. The complicated configurational and spin domain structure might also result in some loss of magnetisation in the domain walls. A further possibility is to consider the influence of the conduction electrons on the Co^{2+} magnetic moment. As mentioned in the Introduction, there is considerable evidence from transport measurements of an important interaction between the localised electrons on the intercalate ions and the conduction electrons, giving rise in particular to a considerable spin-disorder resistivity (Parkin and Friend 1980b), which varies with divalent intercalate ion in a given host TMDC in a way characteristic of the formation

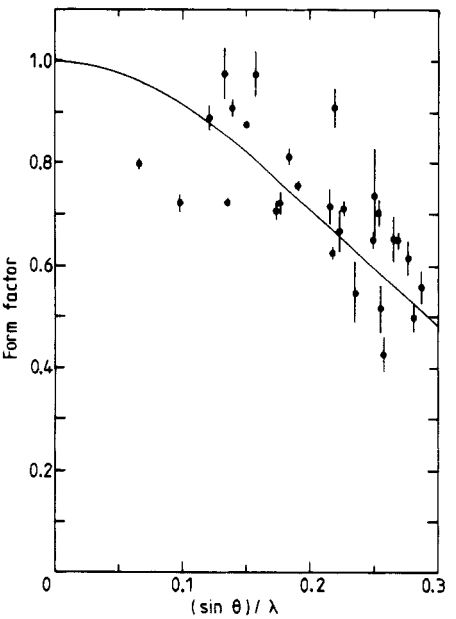

Figure 6. Form factor for the Co ion plotted versus (sin θ)/λ. The full curve corresponds to the calculated form factor of Co^{2+} from Lisher and Forsyth (1971). The points are the measured form factors for the reflections given in table 2.

of Anderson–Friedel virtual bound states on the intercalate ions (see, for example, Gruner and Zawadowski 1978). In such a model, one expects the formation of virtual states with a conduction electron occupying a localised level on the 3d intercalate ion forming, in this case, a Co^{1+} ion. Such a model would give rise to a magnetic moment decreased below that of the Co^{2+} spin-only moment. It is also possible to describe this mechanism in terms of the Co^{2+} ion with the conduction-electron gas locally polarised antiferromagnetically with respect to the Co^{2+} moment, giving a reduced total moment. The response of the conduction-electron gas might be expected to take place over a fairly large length scale and so have an important effect on the form factor only at low (sin θ)/λ. In figure 6, the form factor for Co^{2+} calculated by Lisher and Forsyth (1971) is shown, compared with the experimentally determined form factor for the reflections scanned. At low angles, there appears to be some significant reduction in the measured form factor below that expected which is in agreement with some polarisation of the conduction-electron gas. It is clear, however, that such a conclusion is speculative and further measurements are required.

3.2. $Co_{1/3}TaS_2$

Experiments on this compound were made only at the AERE. A number of reflections were calculated for $Co_{1/3}TaS_2$ based on the orthohexagonal structures mentioned above, but no measurable magnetic intensity was detected at 4.2 K and it was thus necessary to consider other possible structures.

The distribution of Co atoms in $Co_{1/3}TaS_2$ is identical with that of the manganese atoms in the rare-earth manganites, $RMnO_3$ (R = rare earth) and in other ways, their structures are similar (Bacon 1975). In particular, the planes of Mn atoms (which also

contain O atoms) are separated by triple-layer sandwiches of RO_2. The rare-earth manganites are antiferromagnetic materials with Néel temperatures in the range 70–120 K (Koehler *et al* 1964) and adopt a non-collinear triangular antiferromagnetic structure where the magnetic moments on the Mn atoms are directed along three directions at 120° to each other within the basal plane.

The distribution of metal atoms in the nickel arsenide structure is not unrelated to that of the Co atoms in $Co_{1/3}TaS_2$ and the Mn atoms in $RMnO_3$. Hirone and Adachi (1957) examined the magnetic properties of the NiAs structure and showed that, within the molecular-field approximation, triangular spin arrangements can be stable, depending on the relative strengths of the first-, second- and third-nearest-neighbour exchange

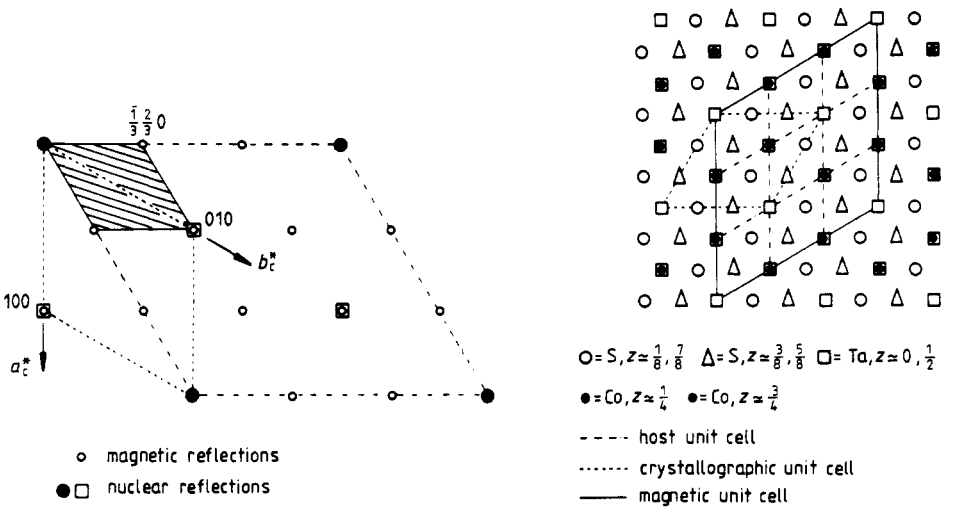

Figure 7. Magnetic unit cell determined for $Co_{1/3}TaS_2$ on the basis of more than twenty weak reflections.

interactions. Subsequently, Corliss *et al* (1961) found a similar magnetic structure in CrSe.

For these reasons, a possible triangular antiferromagnetic structure in $Co_{1/3}TaS_2$ was considered. Figure 7 shows the magnetic reciprocal lattice corresponding to such a structure as compared with the crystallographic lattice for $Co_{1/3}TaS_2$. We have found more than twenty magnetic peaks corresponding to the magnetic lattice shown in figure 7 which have determined that the volume of the magnetic unit cell in real space is indeed three times that of the crystallographic cell.

4. Conclusions

We have determined the magnetic structure of the antiferromagnetic compound, $Co_{1/3}NbS_2$ at 4.2 K using single-crystal photographic and photon-counting techniques. The magnetic structure is relatively simple; the orthohexagonal magnetic supercell is twice as large as the crystallographic unit cell and contains only two Co atoms. The ordering scheme is that labelled hexagonal ordering of the first kind by Corliss *et al* (1956).

The experimental form factor curve can be fitted with that for a Co^{2+} ion, although there is some evidence, from a diminution of the form factor at low $(\sin\theta)/\lambda$ below that expected, of some delocalisation of the magnetic moment. The size of the Co moment is substantially lower, by 8–10% (and possibly as much as 17% if a lower value for the Co nuclear scattering factor is used) from that of the spin-only Co^{2+} ion; we propose that this is a result of the virtual mixing interaction of the Co 3d electrons and the Nb conduction electrons. Direct evidence for this interaction in the related ferromagnetic compound $Mn_{1/4}TaS_2$ has recently been obtained, by us, from a polarised neutron experiment, which has shown that there is a considerable spin polarisation of the conduction electrons within the TaS_2 layers, a distortion of the spin distribution around the Mn d^5 atoms from spherical symmetry and a 15% reduction of the Mn^{2+} moment below the corresponding spin-only value (Parkin *et al* 1983a,b).

Notwithstanding this interaction, these experiments confirm that the bulk of the magnetisation in $Co_{1/3}NbS_2$ is localised on the Co atoms. Each Co atom has 12 nearest neighbours, with 8 of which it is coupled antiferromagnetically and with 4 aligned ferromagnetically. All 6 next-nearest neighbours are aligned ferromagnetically. The only other antiferromagnetic material in this family of compounds for which the magnetic structure is known in detail is $Fe_{1/3}NbS_2$ which orders according to the hexagonal ordering of the third kind scheme. It may be significant that for both this compouund and $Co_{1/3}NbS_2$ the number of parallel and antiparallel nearest neighbours is the same.

We have determined that the magnetic structure of $Co_{1/3}TaS_2$ is very different from that of the Co and Fe intercalates of NbS_2. The material has a $3^{1/2} \times 3^{1/2}$ magnetic supercell which corresponds to a triangular antiferromagnetic structure, which is a relatively uncommon structure. We propose to investigate this material in more detail. The comparison of these magnetic structures and others within this family will be important in gaining further understanding of the wide range of magnetic behaviour shown by these materials.

Acknowledgments

We thank Dr A F Wright for help with the D12 experiment and Dr J B Forsyth and Dr G L Squires for advice and encouragement. We thank Mrs S Nulsen for preparing the samples used in these experiments. We acknowledge support from the SERC.

References

Anzenhofer K, van den Berg J M, Cossee P and Hell J N 1970 *J. Phys. Chem. Solids* **31** 1057

Bacon G E 1975 *Neutron Diffraction* (Oxford: Clarendon)

van den Berg J M 1976 *Physics and Chemistry of Materials with Layered Structures: Optical and Electronic Properties* ed. P A Lee (Dordrecht: Reidel)

Bertaut E F and Mercier M 1963 *Phys. Lett.* **5** 27

Bertaut E F, Pauthenet R and Mercier M 1967 *Phys. Lett.* **18** 13

Brown P J 1978 *Electron and Magnetization Densities in Molecules and Crystals* ed. P Decker (New York: Plenum) p 255

Corliss L, Elliott N and Hastings J M 1956 *Phys. Rev.* B **104** 924

Corliss L, Elliott N, Hastings J M and Sass R L 1961 *Phys. Rev.* **122** 1402

Eibschutz M, De Salvo F J, Hull G W J and Mahajan S 1975 *Appl. Phys. Lett.* **27** 464

Friend R H, Beal A R and Yoffe A D 1977 *Phil. Mag.* **35** 1269

Goodenough J B 1963 *Magnetism and the Chemical Bond* (New York: Wiley)

Gruner H and Zawadowski A 1978 *Progress in Low Temperature Physics* vol 7B (New York: Academic Press)
Hirone T and Adachi K 1957. *J. Phys. Soc. Japan* **12** 156
Hohlwein D and Wright A J 1981 *J. Appl. Crystallogr.* **14** 82
Koehler W C, Yakel H L Wollan E O and Cable J W 1964 *Phys. Lett.* **9** 93
Koester L, Knopf K and Waschkowski W 1974 *Z. Phys.* **271** 201
van Laar B, Rietveld H M and Ijdo D J 1971 *J. Solid State Chem.* **3** 154
Le Blanc-Soreau A, Rouxel J, Gardette M and Gorochov O 1976 *Mater. Res. Bull.* **11** 1061
Lisher E J and Forsyth J B 1971 *Acta. Crystallogr.* A **27** 545
Parkin S S P 1980 *PhD Thesis* University of Cambridge
Parkin S S P *et al* 1983a to be submitted
Parkin S S P and Bayliss S C 1982 *J. Phys. C: Solid State Phys.* **15** 6851–6
Parkin S S P and Beal A R 1980 *Phil. Mag.* **42** 627
Parkin S S P and Friend R H 1980a *Phil. Mag.* **41** 65
—— 1980b *Phil. Mag.* **41** 95
Parkin S S P, Marseglia E A and Brown P J 1983b *J. Phys. C: Solid State Phys.* **16** 2749–64
Wright A F, Berneron M and Heathman S P 1981 *Nucl. Instrum. Methods* **180** 655